International Journal of Pharmaceutics 637 (2023) 122905

Contents lists available at ScienceDirect

International Journal of Pharmaceutics

journal homepage: www.elsevier.com/locate/ijpharm

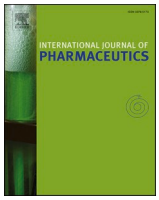

In depth characterization of physicochemical critical quality attributes of a clinical drug-dendrimer conjugate

Silvia Sonzini [a,*], Fanny Caputo [b,c,1], Dora Mehn [d], Luigi Calzolai [d], Sven Even Borgos [b], Astrid Hyldbakk [b], Kevin Treacher [e], Weimin Li [a], Mark Jackman [a], Najet Mahmoudi [f], M. Jayne Lawrence [g], Claire Patterson [h,2], David Owen [i,3], Marianne Ashford [h], Nadim Akhtar [e]

[a] Advanced Drug Delivery, Pharmaceutical Sciences, R&D, AstraZeneca, Cambridge, UK
[b] Department of Biotechnology and Nanomedicine, SINTEF Industry, Trondheim, Norway
[c] Univ. Grenoble Alpes, CEA, LETI, F-38000 Grenoble, France
[d] European Commission, Joint Research Centre (JRC), Ispra, Italy
[e] New Modalities & Parenteral Development, Pharmaceutical Technology & Development, Operations, AstraZeneca, Macclesfield, UK
[f] Rutherford Appleton Laboratory, ISIS Facility, Science and Technology Facilities Council, Didcot OX11 0QX, UK
[g] Division of Pharmacy & Optometry and the North West Centre for Advanced Drug Delivery (NoWCADD), School of Health Sciences, University of Manchester, Oxford Road, Manchester M13 9PL, UK
[h] Advanced Drug Delivery, Pharmaceutical Sciences, R&D, AstraZeneca, Macclesfield, UK
[i] Starpharma Pty Ltd., 4-6 Southampton Cresent, Abbotsford, Victoria 3067, Australia

ARTICLE INFO

Keywords:
Nanomedicine
Nanoparticle
Drug-dendrimer conjugate
Drug delivery
Physicochemical properties

ABSTRACT

A deep and detailed understanding of drug-dendrimer conjugates key properties is needed to define the critical quality attributes that affect drug product performance. The characterization must be executed both in the formulation media and in biological matrices. This, nevertheless, is challenging on account of a very limited number of suitable, established methods for characterizing the physicochemical properties, stability, and interaction with biological environment of complex drug-dendrimer conjugates. In order to fully characterize AZD0466, a drug-dendrimer conjugate currently under clinical development by AstraZeneca, a collaboration was initiated with the European Nanomedicine Characterisation Laboratory to deploy a state-of-the-art multi-step approach to measure physicochemical properties. An incremental complexity characterization approach was applied to two batches of AZD0466 and the corresponding dendrimer not carrying any drug, SPL-8984. Thus, the aim of this work is to guide in depth characterization efforts in the analysis of drug-dendrimer conjugates. Additionally, it serves to highlight the importance of using the adequate complementary techniques to measure physical and chemical stability in both simple and biological media, to drive a complex drug-dendrimer conjugate product from discovery to clinical development.

1. Introduction

The use of nanotechnology for the diagnosis and treatment of diseases is a novel area of research in medicines (Anselmo and Mitragotri, 2016; Shi et al., 2017; Hu et al., 2010). Due to their unique characteristics, drug loaded nanoparticles offer potential to treat a wide spectrum of indications (Anselmo and Mitragotri, 2019). Moreover, nanomedicines can be used in oncology as vectors to deliver a greater proportion of drug to the tumour than what would be possible from systemic exposure. Nanomedicine is a broad term and represents a variety of nanoparticles including liposomes, polymeric nanoparticles, polymer drug conjugates, micelles, iron oxide, silica and gold

Abbreviations: CQA, Critical Quality Attributes; FDA, Food and Drug Administration; EMA, European Medicines Agency; EUNCL, European Nanomedicine Characterisation Laboratory; SOP, Standard Operating Procedure.

* Corresponding author.
E-mail address: silvia.sonzini@astrazeneca.com (S. Sonzini).
[1] Current affiliation: French Metrology Institute (LNE), 1 Rue Gaston Boissier, 75015 Paris, France.
[2] Current affiliation: Seda Pharma Development Services Ltd., Alderley Edge, UK.
[3] Current affiliation: The University of Queensland, Brisbane QLD 4072 Australia.

https://doi.org/10.1016/j.ijpharm.2023.122905
Received 20 November 2022; Received in revised form 19 March 2023; Accepted 27 March 2023
Available online 31 March 2023

nanoparticles (Mitchell et al., 2021; Stiepel et al.). One class of nanocarriers that is receiving significant attention is dendrimers and drug-dendrimer conjugates. Dendrimers are nano-structured three-dimensional polymeric molecules with a tree-like branching architecture. The monomers layers between each branching node are called "Generations." (Madaan et al., 2014). The molecular weight, size and the number of terminal surface groups increase exponentially with each generation offering flexibility to optimize the drug loading and dendrimer properties. Moreover, the rate of release of the active moiety can be controlled by careful selection of linker chemistry through which the drug is conjugated to the dendrimer (Gupta et al., 2017; Kratz et al., 2008; Martin et al., 1972; Caminade et al., 2005; Ulaszewska et al., 2013; Cutler, 2008). Owing to their ability to improve both physicochemical and pharmacokinetic properties of drugs, dendrimers have been explored in many therapeutic and biomedical applications (Anselmo and Mitragotri, 2016; Tran et al., 2017; Fernández et al., 2021; Mignani et al., 2020).

AZD4320 is a potent dual Bcl-2/Bcl-xL inhibitor that has showed promising efficacy in preclinical studies; yet, the dose limiting cardiovascular toxicity coupled with challenging physicochemical properties prevented its clinical development (Patterson et al., 2021). In order to improve AZD4320 solubility (<1 μg/ml in aqueous buffers at physiological pH) and therapeutic index, a novel five-generation (G5) drug-dendrimer conjugate was designed and named AZD0466. The PEGylated poly-L-lysine dendrimer is based on Starpharma's DEP® dendrimer technology and contains up to a maximum of 32 AZD4320 and 32 PEG molecules (Fig. 1) (Arulananda et al., 2021; StarPharma).

Noteworthy, drug-dendrimer conjugates require particular consideration during development and for regulatory submissions as they do not completely fit either in the small molecule or in the biologics category, but they fall under the Food and Drug Administration (FDA) guidance titled: "Drug Products, Including Biological Products, that Contain Nanomaterials Guidance for Industry"(FDA guidance). This guidance reflects the FDA current thinking on the subject and stresses the need to use complementary characterization approaches when measuring material and drug product properties such as size, polydispersity, morphology and drug release. Additionally, in the case of nanomedicines administrated systemically, the guidance highlights the importance to evaluate the impact of product stability, and thus biocompatibility, induced by the interaction of nanomaterials with human plasma and blood components. In fact, the bound plasma proteins on the nanoparticle surface (bio-corona) may modify nanomedicines biophysical properties, which may in turn affect their safety and efficacy profile (Francia et al., 2020). Overall, these key properties, when defined as critical quality attributes (CQAs), must be fully investigated, and characterized during development, and then tightly controlled throughout drug product lifecycle in order to ensure its consistency. The optimal choice of CQAs to monitor for complex therapeutics like drug-dendrimer conjugates is not obvious. Furthermore, while regulatory documents, such as the European Medicines Agency (EMA) reflection papers and regulatory guidance documents have been published for liposomes (EMA; EMA; EMA), intravenous iron-based nano-colloidal products, and block co-polymer micelle medicinal products (EMA; EMA; EMA), no specific regulatory guidance is available for drug-dendrimer conjugates. Both a recent review and the FDA guidance on drug products that contains nanomaterials have outlined candidate CQAs for general nanomedicines in the clinical context, but also acknowledged the need to adapt the selection of CQAs to specific nanomedicine types and proposed additional characterizations to be considered (Dri et al., 2023; FDA guidance). The complexity of nanomedicines frequently means that no single analytical methods are able to fully provide all relevant information about a given quality attribute. Therefore, access to a suite of multiple orthogonal or complementary advanced characterization technologies is often required to develop process understanding and to implement robust quality control strategies (FDA guidance; ICH Q2). Simon *et al.* recently published a proposed definition for the concepts of orthogonality and complementarity of analytical methods, exemplified in the sizing of nanomedicines, to aid in the selection of the appropriate set of methods (Simon et al., 2023). Orthogonal methods are needed to measure one property or CQA to validate the results by measuring the same property by using different physical principles and compare the results to address unknown bias or interferences. Complementary measurements are used to measure different properties (e.g. size and drug release) to get a better understanding of their correlation and their impact on safety and efficacy of the nanomedicine formulation. This work is, to our knowledge, exploring for the first time the use of orthogonal and complementary methods, as defined by Simon *et al.* to perform an in-depth characterization of the physicochemical CQAs of drug-dendrimer conjugate formulations.

Collaboration with research centres with specialised expertise in nanotechnology characterization may offer an effective way to access both the infrastructure and skills needed to develop tailored standard operating procedures and to perform an in depth characterization of

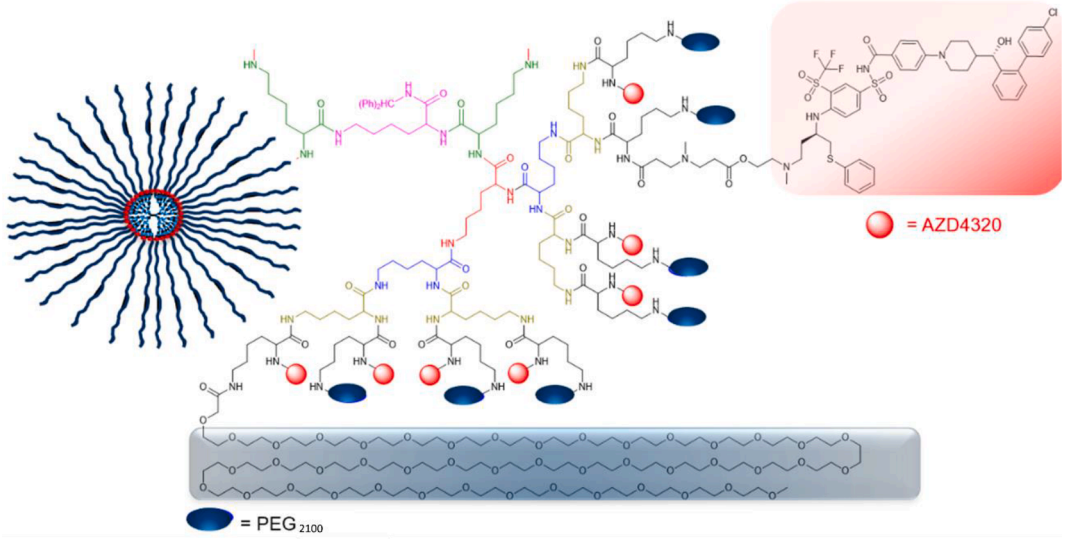

Fig. 1. Tree-like branching architecture of drug-dendrimer conjugate AZD0466. The chemical structures illustrate the poly-Lysine G5, the active small molecule (AZD4320) and the PEG comprising the stealth layer.

these complex systems by comparing the results obtained by multiple characterisation methods. In order to secure access to a wide range of advanced characterization techniques and expertise, a collaboration was initiated between AstraZeneca, Starpharma and European Nanomedicine Characterisation Laboratory (EUNCL). EUNCL was established under the H2020 research program in 2015 to support the development of nanomedicines in Europe, by providing access to a multi-disciplinary expertise and a comprehensive infrastructure offering a set of preclinical tests (physical, chemical, in-vitro and in-vivo biological testing). EUNCL works closely with US National Cancer Institute Nanotechnology Characterisation Laboratory (NCI-NCL) and supports the stakeholders in their development and clinical translation of nanomedicine formulations. The two laboratories also collaborated with regulatory bodies and metrology institutes, to develop standard operation procedures (SOPs) for the assessment of nanomedicine formulations which are relevant for regulatory purposes. All the SOPs developed by EUNCL and NCI-NCL are published on their website (https://ncl.cancer.gov/resources/assay-cascade-protocols, https://www.euncl.eu/about-us/assay-cascade/). In addition, several articles are available where accumulated knowledge and insight are shared with the scientific community (Caputo et al., 2021; Parot et al., 2020; Leong, 2019; Caputo et al., 2019; Gioria et al., 2018; Mehn et al., 2017; Gioria et al., 2019; Clogston et al., 2019).

Herein, the colloidal properties of two different batches of AZD0466 (Patterson et al., 2021), named C1d and C2a depending on the production campaign, and a blank dendrimer, SPL-8984, were investigated. The latter material has the same architecture and linker of AZD0466 but does not contain the active small molecule. To note, AZD0466 C1d was an early small scale discovery batch whilst AZD0466 C2a was manufactured under good manufacturing practice (GMP) at significantly larger scale using a markedly different synthetic route. The structural characterization of AZD0466 is published elsewhere and not focus of this investigation (Akhtar, 2022).

Owing to the inherent complexity of the drug-dendrimer conjugate, several orthogonal and complementary techniques were applied to characterize AZD0466, with a step-by-step approach, namely: (i) prescreening of the physical properties of the formulations with techniques in batch mode, such as dynamic light scattering (DLS), and Taylor dispersion analysis (TDA). (ii) Advanced and high resolution measurements of size, molecular weight, and physical stability of the formulation by hyphenated fractionation techniques such as size exclusion chromatography (SEC) and asymmetric flow-field flow fractionation (AF4) coupled to online concentration and sizing multi-detectors (MD), as well as analytical ultracentrifugation (AUC). (iii) Determination of morphology of the formulations by transmission electron microscopy (TEM) and small-angle neutron scattering (SANS). Furthermore, as a last step, the physical stability and drug release of the drug-dendrimer conjugates in the presence of plasma proteins was also evaluated.

The techniques herein discussed where evaluated to enable an overall colloidal characterization of a drug-dendrimer conjugate, identify which characterization techniques are more appropriate at each stage of development for this specific family of nanomedicines and, eventually, improve understanding of which properties are potential CQAs for this drug product.

2. Materials and methods

The materials analysed herein were synthesised by Starpharma and AZ and shared with EUNCL for the scope of these analyses. The characterizations were performed both at AZ and in the EUNCL laboratories. The drug-dendrimer conjugate as a molecular entity (drug substance) was additionally analysed by several techniques, including nuclear magnetic resonance, mass spectrometry and reverse phase, size exclusion and supercritical fluid chromatography(Akhtar, 2022). Nevertheless, the aim of this partnership was to focus on drug product CQAs and thus drug substance characterizations are not reported herein.

2.1. Reconstitution procedure

The drug-dendrimer conjugates were stored as powder and reconstituted to 25 mg/mL in reconstitution buffer (acetate 100 mM + 2.5 % w/w glucose, pH 5) unless differently stated.

2.2. Dynamic light scattering (DLS)

DLS analysis was performed on a Malvern Zetasizer Nano ZS instrument (Malvern-Panalytical Ltd.) with back scattering detector (173°). Measurements were made in disposable polymethyl methacrylate (PMMA) semi micro cuvettes and data were collected using Malvern Zetasizer software (v7.11). The measurements were performed immediately after reconstitution in the reconstitution buffer at 20°C, without further dilution of the samples. Additional measurements were performed by batch mode DLS after dilution of the reconstituted samples down to 1 mg/mL in various buffers, including acetate 100 mM + 2.5% w/w glucose (pH 5), 10 mM NaCl and PBS + 10% v/v foetal bovine serum (FBS) at pH 7.4. The latter condition was tested at 37°C.

2.3. Zeta potential measurements

Zeta potential was measured on a Malvern Zetasizer Nano ZS instrument. Prior to the measurements, the reconstituted solutions were further diluted to 10 mg/mL in 10 mM NaCl.

2.4. Automated Taylor Dispersion analysis (TDA)

Sizing by TDA was performed using a Viscosizer TD (Malvern-Panalytical Ltd.) using an uncoated capillary and 25°C run temperature. A 280 nm UV filter was used for AZD0466 batches, whilst a 214 nm filter was applied for SPL-8984. The system was calibrated throughout the experimental runs using a 1 mg/mL caffeine solution in Milli-Q water, as recommended by the manufacturer. All samples, unless otherwise stated, were prepared at 25 mg/mL in 25 mM phosphate/citrate buffer + 5% w/w glucose. SPL-8984 was analysed at 40 mg/mL due to low exctinction coefficient. For each sample, at least six replicates and two independent preparations were analysed. Hydrodynamic radius was calculated based on the diffusion coefficient, obtained from the TDA analysis, via the Stokes-Einstein relationship (Panalytical).

2.5. Multi detector-size exclusion chromatography (MD-SEC)

SEC analysis was performed on a Viscotek TDA302 instrument equipped with a GPCMax autosampler and a detector array consisting of Differential Refractive Index (RI), single wavelength UV, Right Angle (90°) and Low Angle (7°) Light Scattering (RALS/LALS) with laser at 633 nm and Differential Pressure Viscometer (DP) (Malvern-Panalytical Ltd). Sample separation was executed on a single pore size (300 Å) silica column (300 × 7.8 mm) with a modified coating to minimise hydrophobic interactions (PLS3030H, Malvern-Panalytical Ltd.) and column oven was kept at 30 °C. The detector array was calibrated using a single polyethylene glycol (PEG) standard of 24 kDa molar mass and 0.4 dL/g Intrinsic Viscosity (IV) and dn/dc in aqueous media of 0.132 (Malvern-Panalytical Ltd.). Samples were prepared volumetrically in 25 mM phosphate/citrate buffer + 5 % w/w glucose with concentrations at approximately 2 mg/mL. Injection volume was 100 µL. Data was processed using the OmniSEC v4 software. The dn/dc values were determined by using a range of solution concentrations and injecting on to the SEC system, determining RI peak areas and calculating from the RI detector calibration constant. Values for dn/dc for the SEC analyses were similar to those determined via the AF4 of the samples (0.151 for AZD0466 C1d and C2a, 0.142 for SPL-8984). Hydrodynamic radius was calculated from the molecular mass and IV via the Stokes-Einstein relationship (Armstrong et al., 2004).

2.6. Multidetector-Asymmetric flow field flow fractionation (MD-AF4)

MD-AF4 analysis was performed using an Eclipse AF4 (Wyatt Technology). The platform included isocratic pump(s), degasser, injector, and a trapezoidal long fractionation channel. Online detectors in the MD-AF4 configuration used were, in order: UV–VIS absorbance, multi-angle light scattering (MALS) with a Wyatt QELS (Quasi-Elastic Light Scattering) integrated directly with the MALS at an angle of 99.9°, and a refractive index detector (dRI). The dRI was used as the concentration detector of reference for molecular weight (MW) determination. The dn/dc was measured in batch mode by direct injections of the samples into the dRI detector (Caputo et al., 2019). The following dn/dc average values (standard deviation, SD) were derived by three replicate measurements and used in the calculation of MW performed by MALS: AZD0466 C1d = 0.155 (0.001); AZD0466 C2a = 0.158 (0.001); SPL-8984 = 0.137 (0.01). Prior to the MD-AF4 analysis, the samples were diluted to 2.5 mg/mL (AZD0466 C1d, AZD0466 C2a) or to 10 mg/mL (SPL-8984) in the reconstitution buffer and tested at 20°C. For the physical stability analysis in complex biological media, the samples were diluted in PBS + 10% v/v FBS and then incubated at 37 °C for 1 h prior to sample injection. The measurement conditions for MD-AF4 analysis are summarized in Table S1. Method precision was evaluated under repeatability conditions at a minimum as described by ISO/TS 21362:2018 (ISO ISO/TS, 2018) (same analyst, same instrument, same location, same method over a short period of time), by performing three replicate injections of each sample. The three replicate fractograms measured for each sample are reported in Fig. S2. Data analysis was performed by Astra v6.1 (Wyatt Technology). Molecular weight values were calculated by applying the Zimm model, with the dn/dc values measured as described above. The hydrodynamic diameter was calculated by a single exponential decay (particle method). The following parameters were reported, as indicated by ISO/TS 21362:2018 (ISO ISO/TS, 2018):

a) Complete fractogram(s), showing the elution time on the x-axis (t_0 = starting of the elution) and the detector response(s) on the y-axis.
b) Molecular weight *vs.* time calculated by applying the Zimm model (1st grade) and the measured dn/dc. The number (Mn), mass (Mw) and centrifugation (Mz) average molar mass and the associated PdI were calculated averaging the MW values across the peak full width half maximum (FWHM).
c) Hydrodynamic radius (Rh) *vs.* time and average Rh across the full width half maximum (FWHM).
d) Measured retention times (Tr) for all identified peaks based on the signal of the UV–VIS detector
e) Mass recovery: in each run absorbance of the eluted fractions was monitored at 320 nm. The amount of mass recovery was estimated by calculating the area under the UV–VIS peak of the samples eluted with and without an applied cross flow:

$$\%mass recovery = \left(\frac{UV-VIS area of the sample}{UV-VIS area of the sample without cross flow}\right)*100;$$

2.7. Analytical ultracentrifugation (AUC)

AUC analysis was carried out overnight using a Beckman Coulter ProteomeLabTM XL-I analytical ultracentrifuge with an 8-hole rotor, at 40,000 rpm, at 20°C. For density estimation the samples were reconstituted at 25 mg/mL concentration in glucose free acetate buffer and suspensions were analysed within 8 h after preparation. Particle size measurements were performed after reconstituting the particles in acetate buffer containing 2.5% w/w glucose and diluting them in the same buffer 250 times for absorbance-based measurements at 325 nm and 25 times for interference-based measurements, respectively. Measurements were performed using sample holders with 2 sector centrepieces. Density of the acetate buffer containing 2.5% glucose was measured using a manual picometer (25 mL) and was found to be 1.011 g/mL at 20°C. Viscosity of the acetate buffer containing 2.5% w/w glucose was determined using an Anton Paar viscometer and was found to be 1.098 mPas at 20°C. Behavior of test samples in the presence of serum was tested after incubation in the presence of 10% v/v FBS at 37°C at 25x dilution (1 mg/mL final concentration).

Measurement of particle density by AUC: Density measurements were performed as previously described (Mehn et al., 2020). Sucrose solutions were prepared in Milli-Q water at concentrations of 20, 25, 30, 35, 40, 50% (% w/w) for AZD0466 and 10, 20, 25, 30, 35% for SPL-8984, respectively. Particle suspensions were diluted 250 times in the sucrose solution and the effect on final sucrose concentration was considered to be negligible. Measurements were performed using a 6 sector centrepiece (running 3 experiments in 1 cell) at 325 nm for AZD0466 and at 220 nm for SPL-8984, respectively. Density of the sucrose solutions was considered to be as reported in TableS2.

2.8. Transmission electron microscopy (TEM)

Prior to TEM measurements (negative staining), the reconstituted samples were diluted to 12.5 mg/mL in Milli-Q water. Sample staining was performed by using Negative Stain-Mica-carbon Flotation Technique (MFT). The samples were absorbed to the clean side of a carbon film on mica, stained and transferred to a 400-mesh copper grid. Sodium Silico Tungstate (SST) $Na_4O_40SiW_{12}$ at 2% w/v in distilled water (pH 7–7.5) was chosen as dye for the analysis of all the samples. The images were taken under low dose conditions (<10 $e^-/Å^2$) with defocus values between 1.2 and 2.5 μm on a Tecnai 12 LaB6 electron microscope at 120 kV accelerating voltage using CCD Camera Gatan Orius 1000. Particle size distribution of AZD0466 C1d and AZD0466 C2a was calculated by manually analysing >400 objects for each sample. Size and shape information were collected by using the Image J software. To get a number-based particle size distribution (PSD), the diameter of an equivalent sphere was calculated by converting the area measured for each event to the equivalent area circle's diameter. The PSD of SPL-8984 was not calculated due to technical issues: despite the staining, the contrast was too low to allow defining the 2D projected area of the particles (even manually).

2.9. Small angle neutron scattering (SANS)

SANS measurements on AZD0466 C1d and C2a were performed on the Sans2d beamline at the ISIS Neutron and Muon Source (STFC Rutherford-Appleton Laboratory, Didcot, U.K.). Sans2d uses a white beam of neutrons with wavelengths, λ, in the range of 1.75–16.5 Å, and the scattering is recorded on two detectors placed at 2.4 and 4 m from the sample, giving an accessible scattering vector range of 0.005–1 $Å^{-1}$. The dendrimer samples were prepared by dissolving AZD0466 at 5 or 10 mg/mL concentration into PBS pH 7.4 prepared with 100% D_2O, then placed in clean, disk-shaped fused quartz cells of 1 or 2 mm pathlength depending on the volume fraction of deuterium in the sample. Size results reported herein are only from samples at 5 mg/mL as the data at 10 mg/mL were within error. The raw SANS data were processed using the Mantid framework (Arnold et al., 2014) following established procedures for the instrument (detector efficiencies, measured sample transmissions, absolute scale using the scattering from a standard polymer, etc.) (Heenan et al., 1997). The SANS intensity, I(Q), of AZD0466 as a function of the scattering vector, $Q = (4\pi/\lambda)\sin(\theta/2)$, where θ is the scattering angle, was obtained from the total intensity, subtracting the scattering from the buffer. The data were modelled with a core–shell ellipsoid (Berr, 1987) which gave the best fit for the scattering curves when compared to spherical or core–shell spherical models. The aggregates were modelled on the core–shell ellipsoid model which assumes the core of each monomer is localised in the centre of the aggregate, with the PEG layer surrounding the cores. The Guinier approximation was applied to calculate the radius of gyration (R_g) and errors are reported as

SD of the Guinier approximation (Guinier and Fournet, 1955). The least-squares refinements were performed using the SasView software, v5 (https://www.sasview.org/). Model constraints and initial estimates were applied to the fitting parameters based on the size measurements from DLS, TDA and the molecular weight determined by MD-SEC. The background was fixed based on the high Q average intensity and the scale was left as a free parameter; the scattering length density (SLD) of the background solvent was fixed, calculated from the SasView SLD calculator.

2.10. Drug release measurements

Simple media - AZD0466 samples were diluted in phosphate saline buffer (PBS) at pH 7.4 to a target concentration of 770 μg/mL and incubated up to the scheduled sampling times at the desired temperatures, namely 5, 25, 37 and 41.5°C. The concentration was selected based on pre-existing calculations of possible clinical dose and dendrimer drug loading. Samples were taken at the following times (hours): 0, 5, 24, 48, 96 and 168 h, and were immediately diluted 10x in dimethylacetamide (DMA) to prevent further drug release and stored at −20°C until analysis. Before analysis by liquid chromatography coupled with mass spectrometry (LC-MS/MS), samples were diluted in acetonitrile (ACN). Quantification was performed against standard curves of the small molecule AZD4320 prepared in ACN. Stable isotope labelled AZD4320 (13C-d7) was added to all samples and standards and used as internal reference. *Complex media* - The drug release in complex media (human plasma, pooled from three healthy anonymized donors) was performed essentially as described for the simple media above, except only at one temperature, 37°C. Sampling (incubation) times were 0, 4, 24, 48, 96h. DMA addition as previously described, and subsequent dilution in ACN, ensured precipitation of the plasma proteins and concomitant solubilization of the released AZD4320. Total dilutions before analysis (10x in DMA, and then remaining in ACN) were 1000x. All incubation and samplings were performed in triplicate.

3. Results

3.1. Particle size distribution measurements by two orthogonal batch mode techniques: DLS and TDA

As first approach, the bulk size of the samples was analysed by batch mode techniques to exclude major physical instability such as very large aggregates.

By DLS analysis, the particle size distribution (PSD) of AZD0466 C1d and C2a appeared monomodal. The average size and polydispersity values obtained by cumulant analysis (z-ave and PdI) over 10 measurements are reported in Fig. 2a and in Table 1. Both C1d and C2a samples presented a higher average size and a PSD shifting to larger sizes compared to that obtained with the blank dendrimer. The results possibly indicate the presence of multiple populations composed of

Table 1
Summary of the physical characterization of the drug-dendrimer conjugate and the blank dendrimer. Average values (SD) are reported, when multiple replicates are available. Size values by techniques: DLS, TDA: hydrodynamic diameter (D_h), AUC: Stokes diameter (D_{Stokes}), TEM: diameter of an equivalent sphere, SANS: diameter of gyration (D_g). In the case of the molecular weight, the Mw is reported, with the addition of Mn for MD-SEC and AF4. Both for MD-SEC and AF4: average size and molecular values calculated over the FWHM; TEM and AUC: x10, x50 and × 90 from the cumulative distribution of size and MW. D_0 by TEM: derived by the number-based particle size distribution, D_3 by AUC: derived by the volume-based particle size distribution.

Attribute & Measurement		AZD0466 C1d	AZD0466 C2a	SPL-8984
Particle size (nm)	DLS (D_h)	15 (1)	17 (1)	11 (1)
	TDA (D_h)	15 (0.4)	17 (0.4)	11 (0.3)
	MD-SEC (D_h)	15 (1)	17 (1)	11 (1)
	AF4-DLS (D_h)	14 (1)	16 (1)	10 (1)
	TEM ($D_{0,10}$,$D_{0,50}$, $D_{0,90}$)	9, 11, 30	11, 15, 21	na
	AUC (D_{Stokes}) ($D_{3,10}$, $D_{3,50}$, $D_{3,90}$)	8.8, 10, 11	10, 12, 14	6.6, 6.8, 7.0
	SANS (Dg, aspect ratio)	9.8, 1.2	12.0, 1.4	na
Molecular weight* (kDa)	AF4-MALS (Mn, Mw)	322, 347	410, 454	76.4, 75.1
	MD-SEC (Mn, Mw)	275, 305	436, 513	72.6, 79.0
	AUC (Mw_{10}, Mw_{50}, Mw_{90})	244, 341, 535	349, 606, 1038	96, 105, 115
Particle density (g/mL)	AUC	1.13		1.08
Intrinsic viscosity (dL/g)	MD-SEC	0.091	0.082	0.141
Surface charge (mV)	Zeta potential	0.1 (0.3)	0.4 (0.2)	−2.4 (1.1)

*Molecular weight distributions are calculated considering spherical shape for all species.

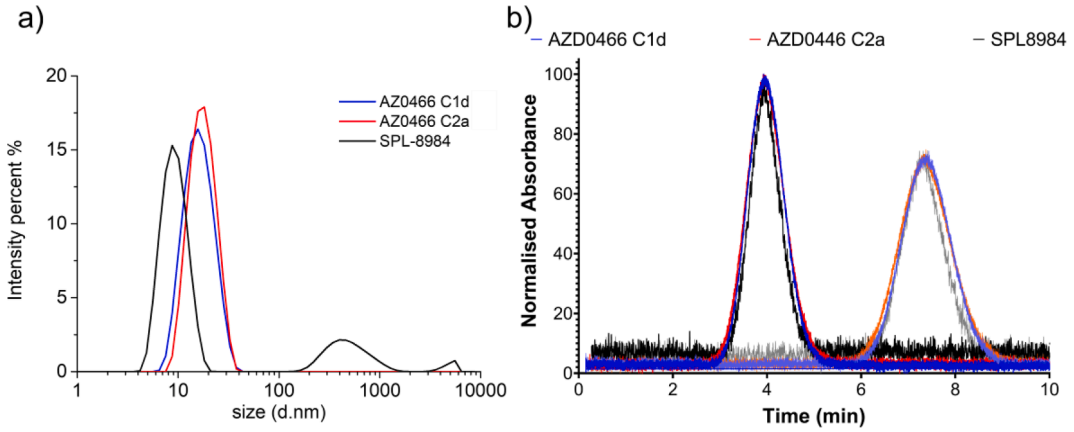

Fig. 2. Pre-screening by batch mode DLS and TDA of AZD0466 and SPL-8984. a) DLS intensity *vs.* size data collected for samples at 25 mg/mL in acetate buffer at 20 °C. b) Normalised TDA Taylorgrams for samples at 25 (AZD0466) or 40 (SPL-8984) mg/mL in citrate buffer at 25 °C; both windows are reported for completeness.

small aggregates (i.e. dimers, trimers) and/or by larger particles which may not be resolved by batch mode DLS. Table S3 reports additional information obtained by the particle size distribution analysis (intensity based), another analytical approach of the DLS correlogram *vs.* the cumulant analysis. As mentioned in previous work (Caputo et al., 2019), a comparison between the two approaches applicable to analyse the DLS data is always useful to get a better understanding of the samples. Usually, if close values are obtained in the two different data treatments, it is indicative of well-monodispersed samples, whereas significantly different values indicate that the sample particle distribution is polydisperse. In this case, the average size values provided by both data analysis approaches were well in agreement for the three drug-dendrimer conjugates. Only in the case of the blank dendrimer (SPL-8984), the intensity-based PSD analysis indicated the presence of a few big aggregates, constituting to 20% of the signal by intensity. No sign of large aggregates was detected in any of the drug-dendrimer conjugates.

Noteworthy, extensive measurements to evaluate size dependency from buffer ions, pH and concentration were performed by DLS. Dilution of the reconstituted samples from 25 mg/mL to 1 mg/mL was executed in various buffers, including PBS with 10% v/v foetal bovine serum (FBS) at pH 7.4; this specific condition was tested at 37°C. Overall, no dependency of size from buffer, pH, concentration, and temperature was noticed (Table S4) allowing the use of slightly different measurement conditions based on each technique requirements.

TDA is a technique used for measuring protein size (Lavoisier and Schlaeppi, 2014) and its usage has also been reported for lysine dendrimers sizing (Cottet et al., 2007). It is orthogonal to DLS, since it is based on a completely different detection principle (TDA based on sample UV absorbance, proportional to sample quantity *vs.* DLS based on intensity of light scattered by the sample, proportional to r^6). On this account, it was selected as a second approach to measure the particle size distribution of SPL-8984, AZD0466 C1d and C2a batches. The TDA Taylorgrams for the first and second reading window are reported in Fig. 2b, showing reproducible profiles. According to the Taylor Dispersion Analysis of the obtained curves (Latunde-Dada et al., 2016; Latunde-Dada et al., 2015; Latunde-Dada et al., 2015), the three AZD0466 batches showed a larger average hydrodynamic diameter (Dh) compared to the blank dendrimer, SPL-8984, in agreement with the DLS data reported above (Table 1). The obtained Dh values are comparable with the DLS measurements, providing a confirmation of the previously obtained sizing results.

Additionally, the particle surface charge was analysed. The average zeta potential values over five measurements and the average zeta potential distribution of the four samples analysed are reported in Table 1. All the samples presented a net neutral surface charge.

3.2. *In depth physical characterization by complementary techniques with online multi-detector measurement settings: MD-SEC, MD-AF4 and AUC*

Once the bulk properties of the drug-dendrimer conjugate samples were analysed by batch-techniques, as second step, complementary hyphenated approaches were used to obtain an in depth understanding of the physical properties of the drug-dendrimer conjugates. Three approaches were selected: (i) SEC coupled with UV–Vis, static light scattering (RALS/LALS), refractive index (RI) and differential viscometer (DP) detectors (ii) AF4 coupled with UV–VIS, multiangle light scattering (MALS), RI and DLS detectors and (iii) AUC equipped with UV–VIS and refractive index detectors. The MD-SEC and MD-AF4 represent complementary methods to first fractionate particles according to their physical properties (size and shape), and then to estimate molecular weight and particle size of the eluted fractions online. AUC is a true orthogonal technique that allows determination of the size of particles based on their sedimentation velocity under the application of a centrifugal force.

The single MD-SEC measurements are reported in Fig. S1, where an overlay of representative chromatograms from the multi-detectors used for analysis (RI, RALS/LALS, DP) is shown for each of the samples. The measurements of the different samples organised by detector are then overlayed in Fig. 3 and a summary of the results is reported in Table 1 and Table S5. The hyphenation of sample fractionation followed by online measurements allows to resolve the presence of different species in the samples. It is worth noting that both the RALS and LALS responses were identical in shape, indicating that all the species in the eluted range, as anticipated, are isotropic scatterers and therefore below the critical size (radius ~ 1/20 of the laser wavelength 633 nm ≈ 31 nm) where the Rayleigh scattering theory is applicable(Kato et al., 2018).

The blank dendrimer, SPL-8984, was composed by >90% (from the RI signal) of a main single species eluting at 8.4 mL with a MW of approximately 72 kDa, in line with its chemical structure. Some smaller peaks were also detected at lower retention volume (Vr), i.e. higher MW, these are likely originating from chemically bonded oligomeric species generated during the synthesis of the dendrimer construct. In contrast, both the AZD0466 C1d and C2a showed very low response at an equivalent Vr, indicating that little if any free monomeric species were present in these samples. This infers that the drug-dendrimer conjugate samples were present as physical aggregates in aqueous solution. This hypothesis was confirmed by independent MD-SEC analyses in organic solvent which demonstrated that the drug substance is mainly monomeric in nature (>90% monomer *vs.* higher order species) with molecular weight between 100 and 105 kDa (Akhtar, 2022). Interestingly, whilst the profiles of the AZD0466 drug product samples (Fig. 3a) were relatively broad they also showed pronounced peaks, which may represent different individual oligomeric states. Focusing on the MW analysis in the Vr where most of each sample eluted, the MW measured for AZD0466 C1d ranged between 230 and 350 kDa (Vr between 6.9 and 8.5 mL), suggesting the presence of physical aggregates formed by 2 or 3 molecules; whilst, in the AZD0466 C2a the range was between 250 and 550 kDa (Vr between 6.4 and 8.5 mL), suggesting the presence of physical aggregates up to pentamers. Additionally, in Fig. 3b the viscometric Dh (calculated from the MW and IV of each Vr increment) showed a corresponding trend in size among the various samples. Furthermore, the results for the differential pressure response from the viscometer along with the resultant intrinsic viscosity data *vs.* retention volume are reported in Fig. 3c; the IV did not change throughout elution for the AZD0466 batches but it did for SPL-8984, in contrast to what observed for molecular weight and size. This means that the effective molecular density must be increasing with molecular weight and physical aggregation, and this is likely driven by the presence of the small molecule (AZD4320).

Whilst not strictly applicable to non-linear polymers such as the AZD0466 pegylated dendrimer, plotting the data from the MD-SEC analysis as a Mark-Houwink plot (logIV *vs.* log M) is useful, as it gives information on the conformation and solvent–solute interactions. As shown in Fig. 3d, SPL-8984 occupies a different space in the Mark-Houwink plot in comparison to the AZD0466 samples. The exponent from the Mark-Houwink fit provides some insight into how the intrinsic viscosity relates to molar mass. For typical linear polymers that are able to expand relatively unconstrained with molecular weight in a theta solvent or better, the exponent is 0.5 or higher. For the fit of SPL-8984, the exponent is approximately 0.39, whereas for AZD0466 C1d and C2a the values are 0.17 and 0.13 respectively. Thus, these drug-loaded constructs act as very dense materials, with only a very small increase of intrinsic viscosity with molar mass, whereas the higher molar mass species present in SPL-8984 are more free to interact with the available solvent as they are not hampered in doing so by the very hydrophobic AZD4320 moieties.

As complementary to the MD-SEC approach, the MD-AF4 analyses were also performed on the AZD0466 and SPL-8984 dendrimers samples. A representative fractogram for each sample is reported in Fig. 4, while the average values obtained for sample recovery, molecular weight, and average size (Dh) are summarized in Table 1 and Table S6. The replicate fractograms measured for each sample are shown in

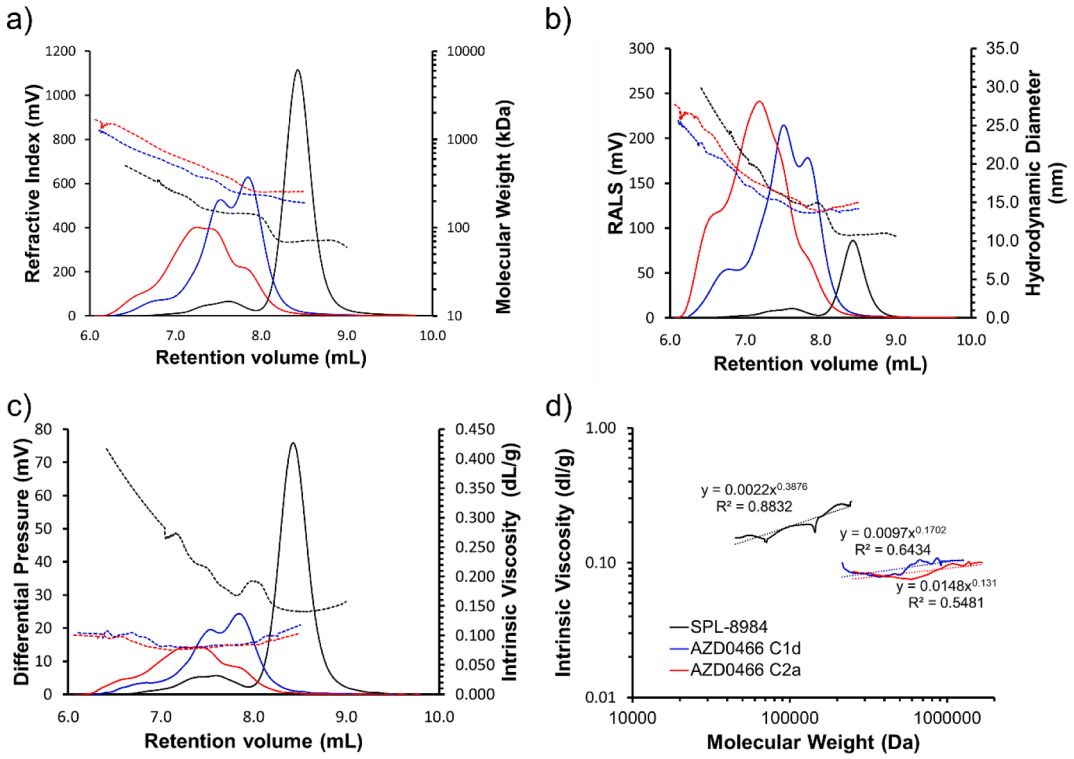

Fig. 3. MD-SEC derived data overlays for SPL-8984 (black), AZD0466 C1d (blue) and C2a (red). a) RI response (solid lines) and molecular mass (dashed lines); b) RALS response (solid lines) and Dh (dashed lines); c) DP response (solid lines) and IV (dashed lines). d) Mark-Houwink type plot for SPL-8984, AZD0466 C1d and C2a; dashed lines are best fit of experimental data. Analyses were carried out reconstituting the samples at 2 mg/mL in 25 mM phosphate/citrate buffer + 5% w/w glucose. (For interpretation of the references to colour in this figure legend, the reader is referred to the web version of this article.)

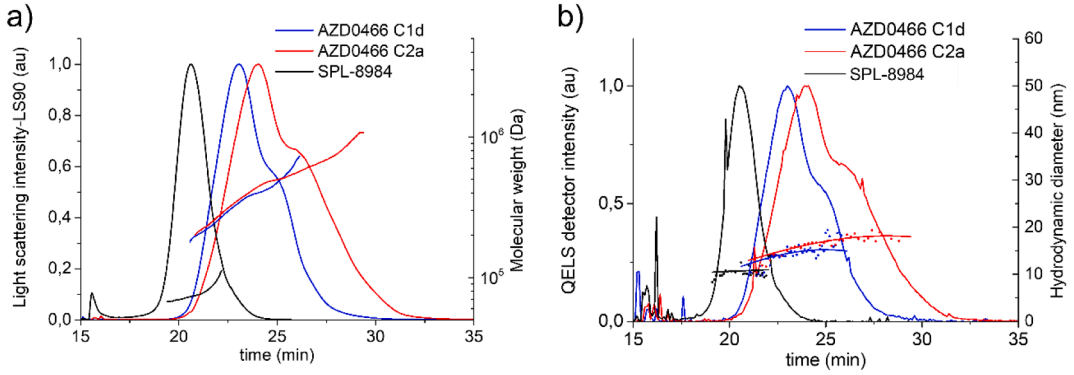

Fig. 4. Overlay of a) molecular weight and b) size by MD-AF4 for SPL-8984 (black), AZD0466 C1d (blue) and C2a (red). Samples were prepared at 25 mg/mL in acetate buffer a diluted to 2.5 mg/mL before analysis. Chromatograms of triplicate analysis are reported in the SI. For both graphs, left-side Y-axis is related to the chromatogram peak solid lines; right-side Y-axis is related to cross-peak solid lines/dots. (For interpretation of the references to colour in this figure legend, the reader is referred to the web version of this article.)

Fig. S2a-c. In line with SEC, also the AF4 fractograms (Fig. 4) indicated that the drug-dendrimer conjugates are composed by multiple species possessing a higher average size and molecular weight than the SPL-8984 blank dendrimer. It is possible to observe a similar but symmetrical elution profile as seen in the MD-SEC analysis, in fact SPL-8984 shows one main single peak and AZD0466 samples show a very broad peak with a shoulder at later time point (elution time is directly correlated to higher MW and larger Dh in this technique, conversely to SEC). As possible to observe in the SEC profiles, whilst the Dh does not vary too much across the peak, the MW is increasing almost in a continuum for both AZD0466 samples, from 100 up to ~ 1000 kDa. The SPL-8984 blank dendrimers have a hydrodynamic diameter (Dh) around 10 nm and molecular weight of around 75 kDa, while the loaded samples AZD0466 C1d and C2a has average diameter of 14 and 16 nm and an average MW of 350 and 450 kDa, respectively. Overall, these results are in agreement with the MD-SEC analysis and further support the presence of small multimers for the drug-dendrimer conjugates samples. Additionally, also in the MD-AF4 analysis the C2a samples were generally composed by larger species and possess a slightly higher polydispersity index (PdI) than AZD0466 C1d (PdI = Mw/Mn). Intriguingly, similar considerations around the MW increase of the drug-dendrimer conjugates *vs.* the blank dendrimer being much more significant than the increase in particle size can be drawn through the AF4 analysis as well as SEC, despite being orthogonal fractionation techniques based on very different separation principles.

Analytical ultracentrifugation can be used to estimate particle

density as already reported in the literature (Mehn et al., 2017). With this aim, sedimentation velocity experiments of the samples were run in different sucrose solutions with density values close to the expected particle density. Particles are expected to sediment in a liquid phase that has a lower density than the particles and float in a medium that has a higher density. As shown in Fig. 5b and Fig. S3, AZD0466 C1d and C2a behaved similarly in the experiments at various sucrose concentrations. They sediment in 25%, float in 35% sucrose, and neither float nor sediment significantly in 30 % sucrose, suggesting they possess a density of about 1.13 g/mL. SPL-8984 has a lower density, similar to the one of 20% sucrose (1.08 g/mL) with negligible sedimentation or floating of the particles being observed during an overnight experiment. Size measurements at 25-fold dilution of the original suspension, using AUC with interference optics (Fig. 5d), resulted in Stokes diameter distributions as shown in Fig. 5a and the correlated molecular weights data as reported in Fig. 5c. Fits were done applying the continuous c(s) model, linear binning, s resolution 200 in the $1 < s < 20$ range. The calculated particle size and molecular weight distributions of the drug-dendrimer conjugates fit well with the results of the analyses performed by orthogonal methods (Table 1). AZD0466 C1d appears to have a particle population with a diameter of about 9 nm and to also contain other small aggregates. The second peak of the particle size distribution appears at 1.16 times the size value of the first peak, suggesting the presence of oligomers in the sample (Mehn et al., 2017). Size distributions of AZD0466 C2a have a mode at about 12 nm and are less resolved, most probably because of the superposition of a wider size distributions of different oligomeric states. SPL-8984 has a smaller size, with a Stokes diameter of about 7 nm and a very narrow particle size distribution. Calculated molecular masses are comparable, if slightly higher than the values determined by MD-SEC and AF4 (Table 1). Measurements at the absorption maximum of the encapsulated drug confirm the absence of free (non-sedimenting) species in the samples. This is further confirmed by the direct measurement of free AZD4320 by LC-MS/MS, which was shown to constitute <1.1% of the total drug (data not shown here). Fig. 5d illustrates the raw data collected by the absorbance optics for the drug loaded particles without background subtraction. The data indicate the absence of a signal of low sedimentation coefficient, small species that would result in a stable absorbance background at the applied rotational speed (40,000 rpm).

3.3. Study of morphology and size by TEM and SANS

To complement the understanding of AZD0466 batches and blank dendrimers properties with morphology information, TEM (in the dry state) and SANS (in solution) were performed. These techniques further enabled additional orthogonal size measurements.

The raw images acquired after negative staining and TEM visualization of the samples, and the derived PSD are reported in Fig. 6, while the calculated diameter values, D_{10}, D_{50} and D_{90} are summarized in Table 1. The samples are all appearing heterogeneous, showing multiple populations: 1) a population of small particles, peaked at 10–15 nm 2) a few larger objects of > 50 nm in diameter and 3) a small amount of aggregates > 200 nm (which were not considered in the analysis of the PSD). On account of the nature of the samples, it was not possible to collect any morphology data. Most of the objects visualized in AZD0466 C2a seems to possess a spherical shape while some of the particles observed in the AZD0466 C1d sample possess a less regular, more elongated shape. Few particles that resembled multimers were detected in AZD0466 C1d, but they represented a very small proportion of the sample population. The TEM observations seem to suggest that the larger particles present in the drug-dendrimer conjugates are mainly associated to the presence of larger and compact objects with a spherical shape. Interestingly the electron contrast of the objects in the 10–15 nm size for the empty dendrimer was much lower than for the drug-dendrimer conjugates. The results are in agreement with MD-SEC, MD-AF4 and AUC analysis of particle intrinsic viscosity and density,

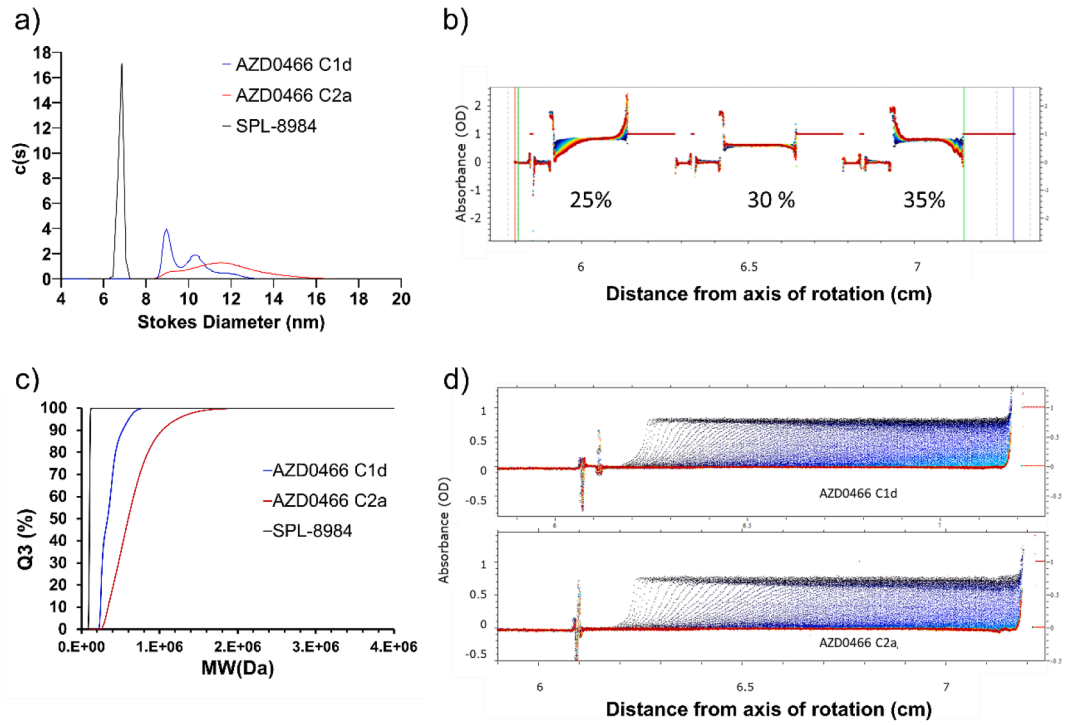

Fig. 5. Particle size distribution, molecular mass, particle density and free *vs.* encapsulated drug estimation by AUC. a) Particle size distribution, b) Example of analysis of particle density (AZD046 C2a): percentage values various represent sucrose concentrations, meniscus on the left, bottom of cell on the right. Various colours represent measurement time points starting from dark blue, ending with red. c) Cumulative molecular mass distribution d) Sedimentation profiles measured at 25-fold dilution (~1 mg/mL), 325 nm, 40,000 rpm. No signal of free, non-sedimenting species is detected at 325 nm. (For interpretation of the references to colour in this figure legend, the reader is referred to the web version of this article.)

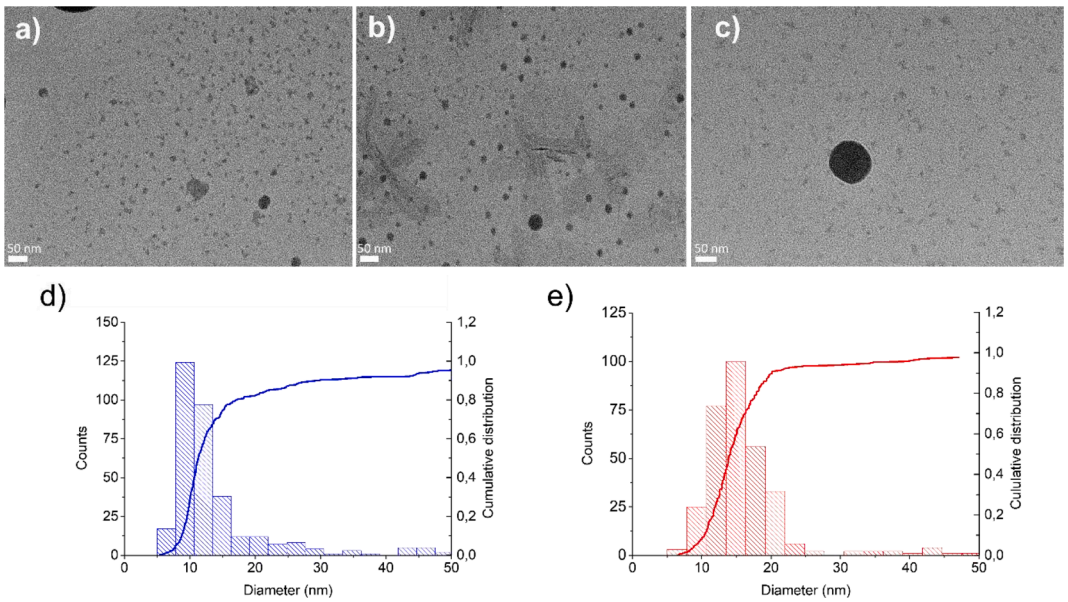

Fig. 6. TEM analysis. Representative images of AZD0466 a) C1d and b) C2a, c) and SPL-8984. Scale bars in the bottom-left corner represent 50 nm. Differential and cumulative PSD of AZD0466 d) C1d and e) C2a. Due to a very low electron contrast, it was not possible to reliably calculate the PSD of the SPL-8984 sample.

further supporting the evidence of a more compact morphology and a higher density of the drug-dendrimer conjugates *vs.* the SPL-8984 blank dendrimer.

In an effort to further understand interactions and self-assembly of drug-dendrimer conjugates, SANS measurements were conducted on AZD0466 C1d and C2a dissolved in deuterated PBS.

AZD0466 was measured in deuterated PBS to obtain the form factor, which is described by a core–shell ellipsoid model as shown in Fig. 7. This model results in the best fit to the scattering curves when compared to spherical or core–shell spherical models. From the fitting reported in Fig. 7, it was possible to calculate a gyration diameter (D_g) of 9.8 nm and 12 nm for AZD0466 C1d and C2a, respectively (Tables 1 and S8). Taking into account the conversion factor from gyration to hydration diameter of 1.3 (Evans and Wennerström, 1999; Tande et al., 2001), these values (12.7 nm and 15.6 nm, respectively) are in line with the hydrodynamic diameter values measured by TDA and DLS (Table 1). To be noted, the same measurements were also performed at 37°C returning values within error (data not shown). Through the fitting, it was also possible to calculate the ellipsoid aspect ratio, revealing a value of 1.2 and 1.4 for C1d and C2a, respectively (Table 1). The complete list of dimensions of the core and shell and respective SLDs are reported in Table S8. Despite the inadequacy of the core–shell ellipsoid model to fully represent the physical self-assembly of dendrimers, this model still gives a good indication on the overall shape in solution. The model also suggests that C2a has slightly higher aspect ratio than C1d, conversely to what observed in TEM in the dry state.

3.4. Physical stability in biological media

As mentioned, physical stability in biological media is an important parameter for nanomedicines (FDA guidance). This characterization generally comprises separation of the drug delivery system from free (not strongly interacting with the nanoparticles) plasma proteins. Although, in the case of drug-dendrimer conjugates, that have sizes comparable to serum proteins, this analysis is particularly challenging as the required separation is not trivial (Åkesson et al., 2012).

Herein, in order to attempt the separation of free serum proteins from the drug-dendrimer conjugates complexed with plasma proteins, AUC and MD-AF4 were selected as characterization techniques comprising online size and molecular weight measurements. AUC can separate plasma components from nanomedicine formulations, such as polymeric particles and liposomes, according to the difference of sedimentation speed between nanoparticles and the free proteins and protein aggregates (Mehn et al., 2020). Unfortunately, in the case of AZD0466, the size and density determining the sedimentation properties of the drug-dendrimer conjugate are too similar to the ones of proteins.

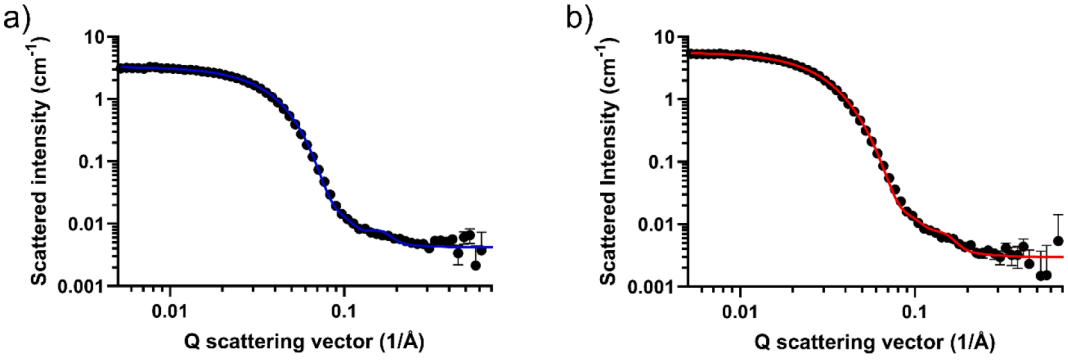

Fig. 7. Scattering curves and geometrical model fitting for AZD0466 C1d and C2a. Scattering curves of C1d (a) and C2a (b). Dots are experimental data. The best fit to the experimental data was obtained using a core–shell ellipsoid model (solid lines). Both AZD0466 batches were dissolved at 5 mg/mL concentration in deuterated PBS at 25°C.

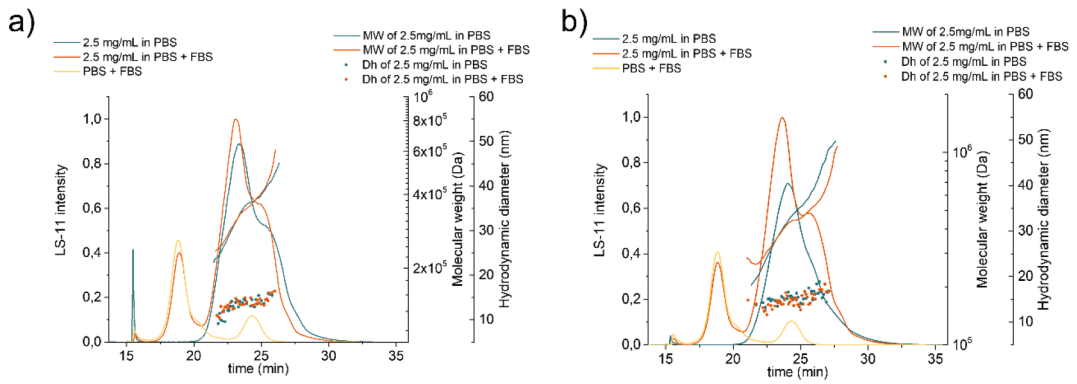

Fig. 8. MD-AF4. Representative fractograms of AZD0466 a) C1d and b) C2a, diluted in PBS (green curves), PBS ± 10% serum (orange curves) and of PBS ± 10% serum alone (yellow curves). Prior to the MD-AF4 analysis, the samples were left incubating 1 h at 37°C. No differences were detected by analysing the particles in PBS with/without incubation at 37°C (data not shown). (For interpretation of the references to colour in this figure legend, the reader is referred to the web version of this article.)

Therefore, it is not possible to separate and distinguish the contribution of the various species in the complex mixture by AUC, unless large aggregates are forming, inducing a significant size difference that may strongly impact the sedimentation coefficient distribution. For the AZD0466 batches, it was not possible to evaluate any change in size in the presence of serum proteins. Additionally, measurements of AZD0466 after incubation in serum, were performed at 325 nm using the AUC absorbance optics (a wavelength specific for absorption of the drug-dendrimer conjugate) to confirm the absence of large aggregates after incubation of AZD0466 in serum. The sedimentation coefficient distribution reported in Fig. S4, does not show any contribution due to large aggregates, suggesting that interaction with plasma proteins does not lead to the formation of large particle aggregates.

AF4 separation was further tested to evaluate dendrimer conjugates physical stability in plasma, in the attempt to obtain a better separation of free plasma proteins and AZD0466, prior to measuring size and molecular weight of the drug-dendrimer conjugates after incubation in serum. The fractograms of the samples incubated in serum are shown in Figs. 8d and S2. Unfortunately, the AF4 fractionation was able to separate the drug-dendrimer conjugates only partially from free serum proteins, since some serum proteins (second peak in the yellow control curves) are eluted at the same time of a portion of the nanoparticle populations (Rt ≈ 24 min). Therefore, in the fractogram of the particles incubated in 10% serum, there is a small shoulder attributed with the presence of free proteins. Nevertheless, by comparing the elution time, MW and D_h values of the samples diluted in PBS with and without serum proteins, it is possible to conclude that, in the specific condition tested, the size and the MW of AZD0466 C1d, C2a and SPL-8984 are not affected by the presence of serum proteins. Thus, it is possible to exclude the presence of strong dendrimer-protein interactions and of aggregation phenomena.

3.5. *In vitro release in buffer and in biological media*

The results presented in the previous section suggest physical stability of AZD0466 batches; nevertheless, even with MD-AF4, complete separation of the drug-dendrimer conjugates from plasma proteins prior to the analysis could not be achieved.

A complementary approach to evaluate drug-dendrimer conjugate behaviour in complex media is to measure the difference in drug release rates of the formulation in simple buffer *vs.* in plasma. In the case of significant interactions of AZD0466 with enzymes differences in release rates could be expected, e.g. accelerated drug release by enzymatic cleavage in plasma *vs*. purely chemical hydrolysis of the ester bonds in simple buffered media. Therefore, to complement the physical stability data, *in vitro* release was analysed as AZD4320 release kinetics from the AZD0466 batches. Incubation in simple buffer of the two drug-dendrimer conjugates batches C1d and C2a and the free drug AZD4320 was performed. Drug release was quantified as concentration of AZD4320 as function of incubation time, measured by LC-MS/MS. First, incubation was tested in simple aqueous media at pH 7.4 (approximating human plasma) and the effect of incubation temperature on drug release kinetics was investigated; the temperatures tested were 4°C, 20°C, 37°C and 41.5°C. The latter temperature point was included as this is very close to the melting point of the drug-dendrimer conjugate (41.6°C) as measured by differential scanning calorimetry

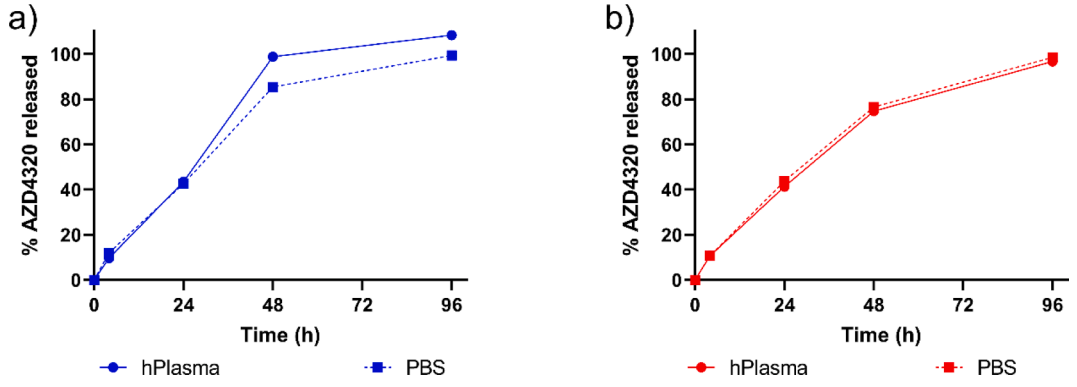

Fig. 9. Drug release experiments in simple and complex media. Percentage (%) of AZD4320 released after incubation at 37°C of the drug-dendrimer conjugates AZD0466 a) Cd1 and b) C2a, up to 96 h. Solid lines represent buffered human plasma and dotted lines PBS pH 7.4. Data in human plasma are N = 3, data in PBS are N = 1.

Table 2
Evaluation of the applicability of techniques tested for the measurement of physical properties of drug-dendrimer conjugates.

Techniques	Bulk/hyphenated or single particle technique	Physical principle	Attributes measured	Applicability for measuring drug-dendrimer conjugates	Simple *vs.* complex media	Simple quality control *vs.* Chain management/drug development
DLS	Bulk	Brownian motion (particle autocorrelation) via light scattering detection	• Dh • PdI • Zeta potential	☑ if PdI < 0.3 ☒ Polydisperse samples or in presence of aggregates.	☑ Simple media ☒ Complex biological media, due to the low resolution	☑ Quality control ☒ Chain management (complementary high resolution assays required)
TDA		Taylor Dispersion Analysis and UV detection combined with Poiseuille flow law	• Dh		☑ Simple media ☑ Complex biological media, due to media baseline subtraction	
MD-SEC	Hyphenation of particle separation + online measurements	Separation based on diffusion through stationary phase hyphenated with multi detectors to measure particle size, molecular weight, and intrinsic viscosity	• Molecular weight • PdI • Size (Dh or Dg) • Intrinsic viscosity	☑ SEC recovery is > 70 %. ☑ DP, MALS and RI allow size measurement ☒ Online MALS is applicable to measure the MW but not particle size due to the small size of the particles	☑ Simple media ☒ Complex biological media, due to interaction with column	☑ Quality control, if easily available and robust method is developed ☑ Chain management/ drug development
MD-AF4		Separation based on diffusion rate dictated by laminar flow hyphenated with multi detectors to measure particle size and molecular weight	• Molecular weight • PdI, • Size (Dh or Dg)	☑ AF4 recovery is > 70 %. ☑ Online DLS is suitable. ☒ Online MALS is applicable to measure the MW but not particle size due to the small size of the particles.	☑ Simple media ☑ Complex biological media	
AUC		Monitoring of particles sedimentation profile by UV–Vis and/or interference optics	• Molecular weight • PdI • Size (Dh or Dg) • Density • Free drug	☑ To obtain sedimentation profile, measure particle density and estimate particle size and molecular weight	☑ Simple media ☒ Complex biological media, since the separation of drug-dendrimer conjugate from free proteins is not possible	
TEM	Bulk, but single particle technique.	Particle visualization by electron contrast in transmission mode	• Morphology • Size • Polydispersity	☑ Drug-dendrimer conjugate ☒ Smaller, less dense blank dendrimer ☒ Morphology hard to define with such small particles	☑ Simple media ☒ Complex biological media	☒ Quality control (expensive, not easily available) ☑ Chain management/ drug development (only technique allowing direct particle visualization)
SANS	Bulk	Measuring elastic neutron scattering at small scattering angles to investigate structures	• Morphology • Crystallinity • Size	☑ Able to identify shape and morphology ☒ Polydisperse samples or in presence of aggregates	☑ Simple media ☒ Complex biological media	☒ Quality control (expensive, not easily available) ☑ Chain management/ drug development (allows complementary structural information)

(data not reported), with a melting curve that showed significant melting characteristics already at temperatures corresponding to physiological fever. The results (Fig. S5) showed a consistently faster release at higher temperatures; drug release was nearly complete after 48 h at the highest temperature tested. No fundamental change in release kinetics was observed at 41.5°C as compared to 37°C, suggesting that the melting of the dendrimer did not significantly affect drug release. Then, drug release in human plasma (pH adjusted to 7.4) was studied at 37°C. The free drug AZD4320 was incubated as a control and no significant degradation of the compound was observed at the time scales studied in this experiment (up to 168 h). Drug release kinetics did not show systematic differences between the two batches (C1d and C2a), and importantly, no significant difference was seen in release kinetics when comparing the simple aqueous medium with plasma, at the same temperature and pH, as shown in Fig. 9 and Figs. S6–S7. The above results indicate that drug release is primarily a function of physicochemical parameters (temperature, pH) and is not significantly accelerated by enzymatic cleavage or otherwise by plasma proteins. Importantly, these results support the assumption that interactions of the analysed drug-dendrimer conjugates with plasma proteins are negligible.

4. Discussion

Drug-dendrimer conjugates, such as AZD0466, are covalently linked

nanoparticles that are widely used in research and development for delivery of drug molecules. Their complex structure and protein-like size pose a significant challenge to both understanding and controlling the CQAs. In order to thoroughly characterize AZD0466 and discern the differences between early batches produced using different manufacturing processes, the colloidal properties of drug-dendrimer conjugates were analysed in the formulation buffer and biological media using multiple orthogonal techniques. The evaluation of the applicability of the techniques tested for the measurement of the physicochemical properties of drug-dendrimer conjugates is summarised in Table 2. Batch techniques such as DLS and TDA enabled a primary understanding of the particle size distribution of the sample, showing significant size differences only between AZD0466 batches and the blank dendrimer. Then, advanced characterization techniques such as MD-SEC, MD-AF4, AUC, TEM and SANS were used for an in depth understanding of the batch-to-batch variability. In the case of MD-SEC and AF4 a fractionation step prior to sizing measurements helped to increase resolution in the determination of the particle size distribution and molecular weight, overcoming some inherent limitations of the batch techniques. These hyphenated techniques were able to discern small differences in molecular weight and physical aggregates formed between the AZD0466 batches, C1d and C2a. Microscopy provided the information at the single particle level and AUC allowed direct measurements of the average particle density. SANS was further able to inform on particles shape, showing that AZD0466 batches are elongated, and not perfect spheres as assumed in all the other solution techniques. Understanding the behaviour of AZD0466 batches in a biological media constituted though the greatest challenge as, currently, no standard analytical solutions exist, so multiple advanced techniques were explored in this work. Unfortunately, none of the available methodologies was able to completely separate the drug-dendrimer conjugates from plasma proteins, as they are of similar size and density. Nevertheless, a partial fractionation was achieved by MD-AF4, allowing a physical stability assessment of drug product performance in presence of plasma proteins. In fact, the measurements in complex media, showed no changes in AZD0466 molecular weight or size, confirming physical stability in biorelevant conditions. Furthermore, the analysis of release rate of the small molecule, AZD4320, in buffer and complex media, with comparable pH and temperature conditions, confirmed that AZD4320 release is only hydrolytically driven. This assay was also able to show similar release profile between AZD0466 C1d and C2a batches, proving that physical aggregation is not impacting AZD4320 release. Therefore, considering the nature of AZD0466 as drug-dendrimer conjugate, many attributes are determined (and controlled) at the manufacturing stage during the chemical synthesis (e.g. in-vitro release *via* linker chemistry, drug-dendrimer conjugate molecular weight *via* controlled chemical synthesis). Therefore, from the overall investigation of colloidal properties, applying a batch method, such as DLS or TDA, as quality control at batch release to test particle size is adequate as there is no evidence that small variation of particle size distribution has a direct impact on drug product performance at this stage. On the other hand, the advanced characterization techniques herein presented could be applied to support equivalence studies in case of future manufacturing changes.

5. Conclusions

The thorough investigation reported herein highlights the necessity, for these complex systems, to design an analytical strategy at the preclinical stage by defining the drug product (and drug substance) CQAs. Based on the information collected, the strategy can be designed into two-layers. A first layer including quality control characterizations to perform on each batch produced, which should be robust, accessible and user friendly analytical methods (e.g. batch methods). Then a second layer combining complementary techniques to apply during early development for drug product and process understanding and later, if process changes are required, to confirm batch equivalence (ICH-Q5E) (EMA ICH). Nevertheless, no standard specifications or methods specifically developed for drug-dendrimer conjugates exist and are available for the community. As future perspective, the authors envisage that the methodologies established during this work could be harmonised and standardised, thus supporting the development of techniques and standards specifically applicable to drug-polymer conjugates. This would allow an easier implementation of the suitable methodologies and relevant expertise in the field, ultimately supporting a faster clinical translation of the most promising drug-dendrimer conjugates to the market.

Author contributions

SS contributed to conceptualisation, data acquisition, analysis, and curation and writing of the manuscript; JL, NM, MJ and WL contributed to SANS data analysis and manuscript writing; KT contributed to MD-SEC data acquisition, analysis, and manuscript writing; NA contributed to conceptualisation and manuscript writing; CP, DO and MA contributed to project conceptualisation. NM and JL contributed to conceptualisation of the SANS experiments and data acquisition. AH and SB contributed to experimental design, data acquisition and analysis of the drug release experiments. FC performed the AF4-MD and TEM analysis, contributed to the experimental design and to manuscript writing. DM designed and performed AUC experiments, contributed to manuscript writing. LC contributed to some experimental design and manuscript writing. All the authors read and approved the manuscript.

Funding sources

FC, DM, LC, SB, AH were supported by the EC as part of the European Nanomedicine Characterisation Laboratory (EUNCL) H2020 project (Grant no. 654190). Experiments at the ISIS Neutron and Muon Source were supported by beamtime allocation from STFC, and the SANS data are available at DOI 10.5286/ISIS.E.RB1820524. This work benefited from the use of the SasView application, originally developed under National Science Foundation Award DMR-0520547. SasView also contains a code developed with funding from the European Union's Horizon 2020 research and innovation program under the SINE2020 project, Grant No. 654000. MJL was also supported by the North West Centre of Advanced Drug Delivery (NoWCADD), a collaborative partnership between the Division of Pharmacy and Optometry, University of Manchester and AstraZeneca (https://www.nowcadd.manchester.ac.uk).

Declaration of Competing Interest

The authors declare the following financial interests/personal relationships which may be considered as potential competing interests: SS, KT, MJ, MA and NA own shares of AstraZeneca. Fanny Caputo, Dora Mehn, Luigi Calzolai, Sven Even Borgos, Astrid Hyldbakk reports financial support was provided by H2020 project (Grant no. 654190). Silvia sonzini, Kevin Treacher, Mark Jackman, Marianne Ashford, Nadim Akhtar reports a relationship with AstraZeneca PLC that includes: employment and equity or stocks. Experiments at the ISIS Neutron and Muon Source were supported by beamtime allocation from STFC, and the SANS data are available at DOI 10.5286/ISIS.E.RB1820524. This work benefited from the use of the SasView application, originally developed under National Science Foundation Award DMR-0520547. SasView also contains a code developed with funding from the European Union's Horizon 2020 research and innovation program under the SINE2020 project, Grant No. 654000.

Data availability

The data that has been used is confidential.

Appendix A. Supplementary material

Supplementary data to this article can be found online at https://doi.org/10.1016/j.ijpharm.2023.122905.

References

European Medicines Agency Reflection paper on the data requirements for intravenous liposomal products developed with reference to an innovator liposomal product. https://www.ema.europa.eu/en/documents/scientific-guideline/reflection-paper-data-requirements-intravenous-liposomal-products-developed-reference-innovator_en.pdf (accessed 19 February 2023).

Åkesson, A., Cárdenas, M., Elia, G., Monopoli, M.P., Dawson, K.A., 2012. The protein corona of dendrimers: PAMAM binds and activates complement proteins in human plasma in a generation dependent manner. RSC Adv. 2 (30), 11245–11248.

Akhtar, N., et al., 2022. The global characterisation of a drug-dendrimer conjugate - PEGylated poly-lysine dendrimer. J. Pharm. Sci.

Anselmo, A.C., Mitragotri, S., 2016. Nanoparticles in the clinic. Bioeng. Transl. Med. 1 (1), 10–29.

Anselmo, A.C., Mitragotri, S., 2019. Nanoparticles in the clinic: an update. Bioeng. Transl. Med. 4 (3), e10143.

Armstrong, J.K., Wenby, R.B., Meiselman, H.J., Fisher, T.C., 2004. The hydrodynamic radii of macromolecules and their effect on red blood cell aggregation. Biophys. J. 87 (6), 4259–4270.

Arnold, O., Bilheux, J.C., Borreguero, J.M., Buts, A., Campbell, S.I., Chapon, L., Doucet, M., Draper, N., Ferraz Leal, R., Gigg, M.A., Lynch, V.E., Markvardsen, A., Mikkelson, D.J., Mikkelson, R.L., Miller, R., Palmen, K., Parker, P., Passos, G., Perring, T.G., Peterson, P.F., 2014. Mantid—data analysis and visualization package for neutron scattering and μ SR experiments. Nucl. Instrum. Methods Phys. Res. A 764 (11), 156–166.

Arulananda, S., O'Brien, M., Evangelista, M., Jenkins, L.J., Poh, A.R., Walkiewicz, M., Leong, T., Mariadason, J.M., Cebon, J., Balachander, S.B., Cidado, J.R., Lee, E.F., John, T., Fairlie, W.D., 2021. A novel BH3-mimetic, AZD0466, targeting BCL-XL and BCL-2 is effective in pre-clinical models of malignant pleural mesothelioma. Cell Death Discov 7 (1), 122.

Berr, S.S., 1987. Solvent isotope effects on alkytrimethylammonium bromide micelles as a function of alkyl chain length. J. Phys. Chem. 91 (18), 4760–4765.

Caminade, A.M., Laurent, R., Majoral, J.P., 2005. Characterization of dendrimers. Adv. Drug Deliv. Rev. 57 (15), 2130–2146.

Caputo, F., Clogston, J., Calzolai, L., Rösslein, M., Prina-Mello, A., 2019. Measuring particle size distribution of nanoparticle enabled medicinal products, the joint view of EUNCL and NCI-NCL. A step by step approach combining orthogonal measurements with increasing complexity. J. Controlled Rel.: Off. J. Controlled Release Soc. 299, 31–43.

Caputo, F., Arnould, A., Bacia, M., Ling, W.L., Rustique, E., Texier, I., Mello, A.P., Couffin, A.-C., 2019. Measuring particle size distribution by asymmetric flow field flow fractionation: a powerful method for the preclinical characterization of lipid-based nanoparticles. Mol. Pharm. 16 (2), 756–767.

Caputo, F., Mehn, D., Clogston, J.D., Rösslein, M., Prina-Mello, A., Borgos, S.E., Gioria, S., Calzolai, L., 2021. Asymmetric-flow field-flow fractionation for measuring particle size, drug loading and (in)stability of nanopharmaceuticals. The joint view of European Union Nanomedicine Characterization Laboratory and National Cancer Institute - Nanotechnology Characterization Laboratory. J. Chromatogr. A 1635, 461767.

Clogston, J.D., Hackley, V.A., Prina-Mello, A., Puri, S., Sonzini, S., Soo, P.L., 2019. Sizing up the Next Generation of Nanomedicines. Pharm. Res. 37 (1), 6.

Cottet, H., Martin, M., Papillaud, A., Souaïd, E., Collet, H., Commeyras, A., 2007. Determination of dendrigraft poly-l-lysine diffusion coefficients by Taylor dispersion analysis. Biomacromolecules 8 (10), 3235–3243.

Cutler, P., 2008. Size-exclusion chromatography. Mol. Biomethods Handbook 719–729.

Dri, D.A., Rinaldi, F., Carafa, M., Marianecci, C., 2023. Nanomedicines and nanocarriers in clinical trials: surfing through regulatory requirements and physico-chemical critical quality attributes. Drug Deliv. Transl. Res. 13 (3), 757–769.

European Medicines Agency Reflection paper on the data requirements for intravenous iron-based nano-colloidal products developed with reference to an innovator medicinal product. https://www.ema.europa.eu/en/documents/scientific-guideline/reflection-paper-data-requirements-intravenous-iron-based-nano-colloidal-products-developed_en.pdf (accessed 19 February 2023).

EMA ICH Q5E Biotechnological/biological products subject to changes in their manufacturing process: comparability of biotechnological/biological products. https://www.ema.europa.eu/en/ich-q5e-biotechnologicalbiological-products-subject-changes-their-manufacturing-process.

Evans, D.F., Wennerström, H., 1999. Chapter 7, Polymers in colloidal systems. In: The Colloidal Domain: Where Physics, Chemistry, Biology, and Technology Meet, 2nd edition ed. Wiley-VCH, p. 672.

Fernández, Y., Movellan, J., Foradada, L., Giménez, V., García-Aranda, N., Mancilla, S., Armiñán, A., Borgos, S.E., Hyldbakk, A., Bogdanska, A., Gobbo, O.L., Prina-Mello, A., Ponti, J., Calzolai, L., Zagorodko, O., Gallon, E., Niño-Pariente, A., Paul, A., Schwartz Jr, S., Abasolo, I., Vicent, M.J., 2021. Vivo antitumor and antimetastatic efficacy of a polyacetal-based paclitaxel conjugate for prostate cancer therapy. Adv. Healthc. Mater., e2101544

Francia, V., Schiffelers, R.M., Cullis, P.R., Witzigmann, D., 2020. The biomolecular corona of lipid nanoparticles for gene therapy. Bioconj. Chem. 31 (9), 2046–2059.

Gioria, S., Caputo, F., Urbán, P., Maguire, C.M., Bremer-Hoffmann, S., Prina-Mello, A., Calzolai, L., Mehn, D., 2018. Are existing standard methods suitable for the evaluation of nanomedicines: some case studies. Nanomedicine (Lond.) 13 (5), 539–554.

Gioria, S., Caputo, F., Mehn, D., 2019. Nano-enabled medicinal products: time for an international advanced community? Nanomedicine (Lond.) 14 (14), 1787–1790.

Guinier, A., Fournet, G., 1955. Small-Angle Scattering of X-Rays. John Wiley & Sons.

Gupta, L., Sharma, A.K., Gothwal, A., Khan, M.S., Khinchi, M.P., Qayum, A., Singh, S.K., Gupta, U., 2017. Dendrimer encapsulated and conjugated delivery of berberine: a novel approach mitigating toxicity and improving in vivo pharmacokinetics. Int. J. Pharm. 528 (1–2), 88–99.

Heenan, R.K., Penfold, J., King, S.M., 1997. SANS at pulsed neutron sources: present and future prospects. J. Appl. Cryst. 30 (6), 1140–1147.

Hu, C.M., Aryal, S., Zhang, L., 2010. Nanoparticle-assisted combination therapies for effective cancer treatment. Ther. Deliv. 1 (2), 323–334.

ICH guideline Q2(R2) on validation of analytical procedures. In: https://www.ema.europa.eu/en/documents/scientific-guideline/ich-guideline-q2r2-validation-analytical-procedures-step-2b_en.pdf.

FDA; CDER; CBER Drug Products, Including Biological Products, that Contain Nanomaterials - Guidance for Industry. https://www.fda.gov/regulatory-information/search-fda-guidance-documents/drug-products-including-biological-products-contain-nanomaterials-guidance-industry.

ISO ISO/TS 21362:2018 Nanotechnologies — Analysis of nano-objects using asymmetrical-flow and centrifugal field-flow fractionation. https://www.iso.org/standard/70761.html.

Kato, H., Nakamura, A., Kinugasa, S., 2018. Effects of angular dependency of particulate light scattering intensity on determination of samples with bimodal size distributions using dynamic light scattering methods. Nanomaterials 8 (9), 708.

Kratz, F., Muller, I.A., Ryppa, C., Warnecke, A., 2008. Prodrug strategies in anticancer chemotherapy. ChemMedChem 3 (1), 20–53.

Latunde-Dada, S., Bott, R., Hampton, K., Leszczyszyn, O.I., 2015. Analytical mitigation of solute–capillary interactions in double detection Taylor Dispersion Analysis. J. Chromatogr. A 1408, 255–260.

Latunde-Dada, S., Bott, R., Hampton, K., Patel, J., Leszczyszyn, O.I., 2015. Methodologies for the Taylor dispersion analysis for mixtures, aggregates and the mitigation of buffer mismatch effects. Anal. Methods 7 (24), 10312–10321.

Latunde-Dada, S., Bott, R., Barker, D., Leszczyszyn, O.I., 2016. Methodologies for the rapid determination of the diffusion interaction parameter using Taylor dispersion analysis. Anal. Methods 8 (2), 386–392.

Lavoisier, A., Schlaeppi, J.-M., 2014. Early developability screen of therapeutic antibody candidates using Taylor dispersion analysis and UV area imaging detection. MAbs 7.

Leong, H.S., et al., 2019. On the issue of transparency and reproducibility in nanomedicine. Nat. Nanotechnol. 14 (7), 629–635.

Madaan, K., Kumar, S., Poonia, N., Lather, V., Pandita, D., 2014. Dendrimers in drug delivery and targeting: drug-dendrimer interactions and toxicity issues. J. Pharm. Bioallied Sci. 6 (3), 139–150.

Martin, J.R., Johnson, J.F., Cooper, A.R., 1972. Mechanical properties of polymers: the influence of molecular weight and molecular weight distribution. J. Macromol. Sci. 8 (1), 57–199.

Mehn, D., Iavicoli, P., Cabaleiro, N., Borgos, S.E., Caputo, F., Geiss, O., Calzolai, L., Rossi, F., Gilliland, D., 2017. Analytical ultracentrifugation for analysis of doxorubicin loaded liposomes. Int. J. Pharm. 523 (1), 320–326.

Mehn, D., Capomaccio, R., Gioria, S., Gilliland, D., Calzolai, L., 2020. Analytical ultracentrifugation for measuring drug distribution of doxorubicin loaded liposomes in human serum. J. Nanopart. Res. 22 (6), 158.

Mignani, S., Shi, X., Rodrigues, J., Roy, R., Muñoz-Fernández, Á., Ceña, V., Majoral, J.-P., 2020. Dendrimers toward translational nanotherapeutics: concise key step analysis. Bioconjug. Chem. 31 (9), 2060–2071.

Mitchell, M.J., Billingsley, M.M., Haley, R.M., Wechsler, M.E., Peppas, N.A., Langer, R., 2021. Engineering precision nanoparticles for drug delivery. Nat Rev Drug Disc 20 (2), 101–124.

Panalytical, M. Understanding Taylor Dispersion Analysis. https://www.malvernpanalytical.com/en/learn/knowledge-center/whitepapers/WP150609UnderstandingTDA.html.

Parot, J., Caputo, F., Mehn, D., Hackley, V.A., Calzolai, L., 2020. Physical characterization of liposomal drug formulations using multi-detector asymmetrical-flow field flow fractionation. J. Control. Release 320, 495–510.

Patterson, C.M., Balachander, S.B., Grant, I., Pop-Damkov, P., Kelly, B., McCoull, W., Parker, J., Giannis, M., Hill, K.J., Gibbons, F.D., Hennessy, E.J., Kemmitt, P., Harmer, A.R., Gales, S., Purbrick, S., Redmond, S., Skinner, M., Graham, L., Secrist, J.P., Schuller, A.G., Wen, S., Adam, A., Reimer, C., Cidado, J., Wild, M., Gangl, E., Fawell, S.E., Saeh, J., Davies, B.R., Owen, D.J., Ashford, M.B., 2021. Design and optimisation of dendrimer-conjugated Bcl-2/xL inhibitor, AZD0466, with improved therapeutic index for cancer therapy. Commun. Biol. 4 (1), 112.

Shi, J., Kantoff, P.W., Wooster, R., Farokhzad, O.C., 2017. Cancer nanomedicine: progress, challenges and opportunities. Nat. Rev. Cancer 17 (1), 20–37.

Simon, C.G., Borgos, S.E., Calzolai, L., Nelson, B.C., Parot, J., Petersen, E.J., Roesslein, M., Xu, X., Caputo, F., 2023. Orthogonal and complementary measurements of properties of drug products containing nanomaterials. J. Control. Release 354, 120–127.

European Medicines Agency Joint MHLW/EMA reflection paper on the development of block copolymer micelle medicinal products. https://www.ema.europa.eu/en/documents/scientific-guideline/draft-joint-ministry-health-labour-welfare/european-medicines-agency-reflection-paper-development-block-copolymer-micelle-medicinal-products_en.pdf (accessed 19 February 2023).

StarPharma. https://www.starpharma.com/drug_delivery/dep_docetaxel.

Stiepel, R.T., Duggan, E., Batty, C.J., Ainslie, K.M. Micro and nanotechnologies: the little formulations that could. n/a (n/a), e10421.
Tande, B.M., Wagner, N.J., Mackay, M.E., Hawker, C.J., Jeong, M., 2001. Viscosimetric, hydrodynamic, and conformational properties of dendrimers and dendrons. Macromolecules 34 (24), 8580–8585.
Tran, S., DeGiovanni, P.J., Piel, B., Rai, P., 2017. Cancer nanomedicine: a review of recent success in drug delivery. Clin. Transl. Med. 6 (1), 44.
Ulaszewska, M.M., Hernando, M.D., Moreno, A.U., García, A.V., García Calvo, E., Fernández-Alba, A.R., 2013. Identification and quantification of poly(amidoamine) PAMAM dendrimers of generations 0 to 3 by liquid chromatography/hybrid quadrupole time-of-flight mass spectrometry in aqueous medium. Rapid Commun. Mass Spectrometry: RCM 27 (7), 747–762.